Rare Metal Materials and Engineering
Volume 52, Issue 9, September 2023
Available online at www.rmme.ac.cn

Science Press

Cite this article as: Gao Zhongtang, Lu Jiawei, Yu Yuan, et al. Effect of W Addition on Microstructure, Mechanical Properties, and Oxidation Behavior of ZrB_2-SiC Composites[J]. Rare Metal Materials and Engineering, 2023, 52(09): 3003-3011.

ARTICLE

Effect of W Addition on Microstructure, Mechanical Properties, and Oxidation Behavior of ZrB_2-SiC Composites

Gao Zhongtang[1], Lu Jiawei[1,2,3], Yu Yuan[2,3,4], Wang Yifei[5], Yu Defeng[1], Li Tongyang[2,3], Wang Lujie[2,4], Tang Huaguo[2,3], Qiao Zhuhui[2,3,4]

[1] College of Mechanical Engineering, Xi'an University of Science and Technology, Xi'an 710054, China; [2] State Key Laboratory of Solid Lubrication, Lanzhou Institute of Chemical Physics, Chinese Academy of Sciences, Lanzhou 730000, China; [3] Shandong Laboratory of Yantai Advanced Materials and Green Manufacture, Yantai 264006, China; [4] Yantai Zhongke Research Institute of Advanced Materials and Green Chemical Engineering, Yantai 264006, China; [5] Northwest Institute for Nonferrous Metal Research, Xi'an 710016, China

Abstract: The ZrB_2-SiC composites with refractory metal W of different contents (1vol%, 3vol%, and 5vol%) were prepared by spark plasma sintering. The densification behavior of composites during sintering process was investigated. The influence of W additions on the microstructure evolution, phase composition, mechanical properties, and oxidation behavior of W-doped composites was studied. Results show that the W addition leads to the formation of core-shell structures in the composites, where the ZrB_2 grains are considered as the core and the in-situ formed (Zr, W)B_2 solid solution is considered as the shell, thereby effectively promoting the grain refinement and composite densification. Compared with those of the W-free composites, the Vickers hardness, flexural strength, and fracture toughness of W-doped composites are enhanced. The optimal mechanical properties can be achieved at W addition content of 3vol%: the highest hardness, strength, and toughness can be obtained for the composites. The mass gain and oxide scale thickness of composites are gradually decreased with increasing the W addition from 0vol% to 5vol%. When the W addition in composite is 5vol%, the SiC-depleted layer disappears. Finally, the influence mechanism of W addition on the performance of composites is discussed.

Key words: ZrB_2-SiC composite; densification; microstructure; mechanical properties; oxidation behavior

Zirconium diboride (ZrB_2) has high melting point (above 3000 °C), high hardness, low density, good thermal stability, and suitable coefficient of thermal expansion, which is usually used as ultrahigh-temperature ceramic in aero-engine, nuclear fission reactor, and high temperature electrode fields[1–3]. Due to its low self-diffusivity and strong chemical bond, ZrB_2 shows poor sintering processibility, inferior fracture toughness, and weak oxidation resistance[4–6]. Recently, the sintering process and sintering additives have been extensively studied to solve the shortages[7–9]. Particularly, the spark plasma sintering (SPS) has been identified as an efficient technique to prepare dense ZrB_2 ceramics owing to the high heating and cooling rates during processing[10–12].

It is known that SiC additive can remarkably improve the fracture toughness by inhibiting the grain growth and optimize the oxidation behavior by promoting the generation of SiO_2 layer[13]. The ZrB_2-SiC ceramics with 5vol%–30vol% SiC are considered to be used in the key parts at ultrahigh temperatures[14–15]. However, the evaporation of B_2O_3 and SiO_2 leads to the active oxidation of SiC and the degradation of oxidation resistance at high temperatures (>1400 °C)[16]. In addition, the complex preparation of dense ZrB_2-SiC ceramics results in the loose microstructure, which has negative effects on the mechanical properties[17]. Therefore, exploring suitable additives in ZrB_2-SiC ceramics is urgently needed to overcome these drawbacks.

Received date: December 07, 2022
Foundation item: National Natural Science Foundation of China (51804251, 52104384); Science Fund of Shandong Laboratory of Yantai Advanced Materials and Green Manufacturing (AMGM2021F04); Shandong Provincial Natural Science Foundation (ZR2021ME168, ZR2021JQ20); Planning Project of Xi'an Science and Technology (21XJZZ0041); LICP Cooperation Foundation for Young Scholars (HZJJ21-07); Taishan Scholars Program of Shandong Province; Youth Innovation Promotion Association (CAS 2021423); Key Research and Development Program of Shaanxi (2023-YBGY-343)
Corresponding author: Yu Yuan, Ph. D., Associate Professor, State Key Laboratory of Solid Lubrication, Lanzhou Institute of Chemical Physics, Chinese Academy of Sciences, Lanzhou 730000, P. R. China, Tel: 0086-29-85583157, E-mail: yuyuan@licp.cas.cn

The refractory metal W and W-based phases have great potential in ZrB_2-based composites. Adding W-based phase can exert positive effects on the comprehensive properties of ZrB_2-based composites[18]. The WC addition (5vol%) can promote self-accelerated diffusion processes and enhance densification by the formation of core-shell structure during sintering[19]. WC addition increases the viscosity and density of the oxide scale owing to the formation of ZrO_2-WO_3 eutectic structure, which results in the reduction in oxygen diffusion rate of the interior material[20]. WB addition can also ameliorate the oxidation behavior of materials due to the active oxidation of WB[21]. In addition, adding metals (Ni, Mo, Nb, Zr, and Al) can effectively improve the densification of ZrB_2-based composite and remove the oxide impurities of ZrB_2 particles through the formation of liquid phase in sintering process[22–24]. Ding et al[25] reported that the W can enhance the mechanical properties by ZrB_2 grain refinement and solid solution strengthening in W-doped ZrB_2 ceramics. A large number of studies investigate the positive functions of refractory metal W on property enhancement of ZrB_2-based ceramics. Therefore, the addition of refractory metal W is also expected to improve the comprehensive properties of ZrB_2-SiC-based ceramics, such as mechanical behavior and oxidation behavior. However, the function of direct addition of metal W in ZrB_2-SiC-based composites is rarely investigated.

In this research, the ZrB_2-SiC-based ceramics with W addition of different contents were sintered by SPS. The densification behavior of composite was evaluated by analyzing the sintering process of W-doped composites. The microstructure evolution and phase composition of the composite were analyzed. The mechanical behavior and oxidation behavior of W-doped composites were evaluated and the influence mechanism of W additions was discussed. This research provided theoretical guidance for the effect of function optimization of refractory metal W on enhancement in densification behavior, mechanical behavior, and oxidation behavior of ZrB_2-SiC-based ceramics.

1 Experiment

The original ZrB_2 powder (purity>99.9%, average particle size<200 nm), SiC powder (purity>99.5%, average particle size <200 nm), and W powder (purity>99%, average particle size<1 μm) were purchased from Changsha Tianjiu Co., Ltd, China. In order to obtain the powder mixtures, the specimens containing 80vol% ZrB_2-20vol% SiC powder and W addition of 0vol% , 1vol% , 3vol% , and 5vol% were prepared by electromagnetic stirring in ethanol for 8 h, and they were named as ZS-0, ZSW-1, ZSW-3, and ZSW-5, respectively. The mixture was dried at 80 °C for 24 h in a vacuum drying oven. Then, the powder mixtures were sieved at <200 μm to remove the ethanol. Finally, the resultant powder was sintered by SPS under the conditions of holding temperature of 2100 ° C, temperature preservation time of 10 min, and uniaxial pressure of 50 MPa in the vacuum environment. After SPS process, the sintered specimens were cooled down to 700 °C within 10 min under uniaxial pressure of 50 MPa, and then the sintered composites were naturally cooled down. The temperature and loading head displacement were simultaneously recorded.

The densities of sintered composites were calculated by Archimead method with distilled water as immersion medium. The microstructure evolution of the sintered specimens was characterized via scanning electron microscope (SEM, JSM-5600 L), the energy dispersive spectrometer (EDS), and the X-ray diffractometer (XRD, Bruker D8) with scanning rate of 2°/min. The grain size was estimated by the commercial software Image Pro Plus. Vickers hardness was determined via the Vickers hardness tester (THVS-50) at the load of 5 kg (49 N) and head holding time of 20 s. The three-point bending tests were used to test the flexural strength on the universal testing machines (Instron 1195). The size of test specimen was 3 mm×4 mm×25 mm, the crosshead speed was 0.5 mm/min, and the span was 20 mm. The fracture toughness was estimated by the direct crack measurement method on Vickers hardness testing machine, the test load (L) was 5 kg (49 N), and the head holding time was 20 s. The half radial crack length (C) was measured by SEM. Finally, the value of fracture toughness (K_{IC}) was obtained by Anstis formula[22], as follows:

$$K_{IC} = 0.016\left(\frac{E}{H_V}\right)^{1/2}\left(\frac{L}{C^{3/2}}\right) \quad (1)$$

where E and H_V are elastic modulus and hardness, respectively. Elastic modulus can be obtained by Nielsen formula[26], as follows:

$$E = E_0\frac{(1-p)^2}{1+(\rho^{-1}-1)^p} \quad (2)$$

where E_0 is the elastic modulus of the fully-densified specimen; p is the volume content of pores; ρ is the Nielsen shape factor (0.4).

The size of the sintered specimens was 4 mm×4 mm×15 mm, and all sides of the specimens were polished. The specimens were oxidized in a high-temperature muffle furnace. The maximum temperature and holding time were 1500 °C and 2 h, respectively. Then, the oxidative specimens were naturally cooled. The mass gain Δm (over the exposed area) of specimen was recorded by the electronic balance. The microstructures and thicknesses of the oxide layer were characterized and calculated by SEM-EDS according to the cross-section of oxidized specimens. The specimens were tested at least three times to ensure the evaluation accuracy of mechanical and oxidation properties.

2 Results and Discussion

2.1 Densification and microstructure

The variation trends of displacement and temperature of ZS-0 and ZSW-3 specimens are shown in Fig. 1. The initial amount of powder is sufficient for the preparation of fully-densified specimen with thickness of 5 mm and diameter of 30 mm. The initial external load (20 MPa) gradually increases to 50 MPa within 4 min after the initiation of SPS process.

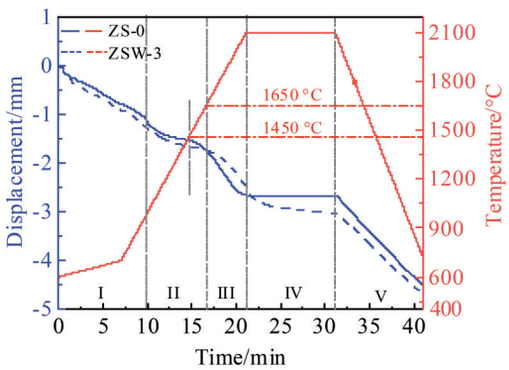

Fig.1 Temperature and displacement of ZS-0 and ZSW-3 specimens during SPS process

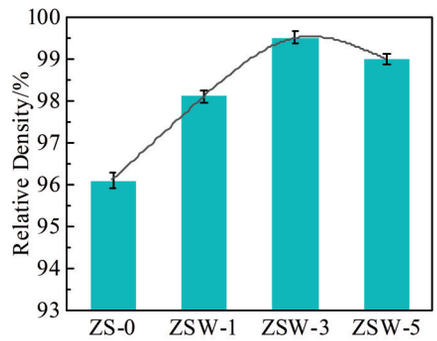

Fig.2 Relative density of SPS-treated specimens with different W contents

The sintering furnace is heated to 2100 °C with heating rate of 100 °C/min, and the infrared thermometer starts recording at above 600 °C.

As shown in Fig. 1, the sintering process of both ZS-0 and ZSW-3 specimens contains five stages. The sintering displacement of two specimens is decreased due to the particle rearrangement in the first stage. Due to the complementary influence of sintering consolidation-shrinkage and thermal expansion of powders in the second stage, the absolute value of slope of displacement curves of two specimens is decreased. In the third stage, the absolute value of slope of sintering displacement curve is significantly increased and therefore the sintering displacement is sharply decreased, which is attributed to the dominant position of sintering consolidation-shrinkage phenomenon. It is reported that the addition of refractory sintering additives can increase the sintering consolidation-shrinkage temperature of boride ceramics[27]. In this research, the consolidation-shrinkage temperature of ZS-0 and ZSW-3 specimens is 1450 and 1650 °C, respectively. The W addition increases the consolidation-shrinkage temperature of ZrB_2-SiC specimen. The sintering displacement of ZS-0 specimen is almost unchanged in the fourth stage, i.e., the densification process stops at the temperature preservation stage. This is because a large number of available sintering driving forces are consumed by the matrix growth in high-temperature sintering at 2100 °C. Contrastingly, the sintering displacement of W-doped ZSW-3 specimen is still significantly decreased in the fourth stage, indicating that the W addition improves the sintering driving force for further densification, so the densification process of W-doped specimens can be continued. The sintering displacement curve decreases obviously in the final stage, owing to the thermal expansion and contraction effect in the cooling stage. The ZSW-3 specimen exhibits higher shrinkage value (4.78 mm) than the ZS-0 specimen (4.50 mm) does, which further reveals the importance of W addition on the densification behavior of ZrB_2-SiC-based composites.

The relative density of the specimens with different W contents is shown in Fig. 2. The relative density of ZS-0 specimen without W addition is 96.1%, whereas that of ZSW-1, ZSW-3, and ZSW-5 specimens with W addition is all higher than 98%. The ZSW-3 specimen exhibits the highest relative density of about 99.5%. Therefore, the introduction of W element can significantly promote the densification of W-doped composites.

XRD patterns of different specimens are shown in Fig. 3. The dominant phases (ZrB_2 and SiC) can be identified in all specimens. It is worth noting that no W peaks can be observed for the W-doped specimens, whereas the diffraction peaks of in-situ formed WB phase can be identified. According to the diffraction peaks, the diffraction peak intensity of WB phase is significantly enhanced with increasing the W content from 1vol% to 5vol%. The enlarged XRD pattern of ZrB_2 is shown in the inset of Fig. 3. It is obvious that the position of ZrB_2 peak shifts to the higher 2θ region after W addition, suggesting that the W addition in ZrB_2-SiC-based composites results in the decrease in ZrB_2 lattice parameters. This phenomenon also indicates the formation of solid solution phases during SPS process. The lattice distortion is related to the mixture of ionic and covalent bonds in the generation of solid solution phases[28]. The decrease in ZrB_2 lattice parameters should be associated with the dissolution-diffusion behavior in densification process of composites, as shown in Fig.1.

SEM morphologies of polished surfaces of ZS-0, ZSW-1,

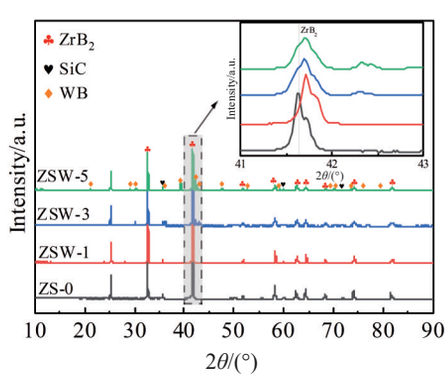

Fig.3 XRD patterns of SPS-treated specimens with different W contents

ZSW-3, and ZSW-5 specimens are shown in Fig.4. The bright phase and dark phase in Fig. 4a represent the ZrB_2 grain and SiC grain, respectively. According to XRD results, the white phase is WB phase, as shown in Fig. 4b–4d. The porosity of specimens with W addition is significantly lower than that without W addition. The specimen without W addition exhibits loose grain structure and inferior intergranular adhesion, whereas those with W addition exhibit relatively dense microstructures. The pores are mainly distributed at the grain boundaries and triple junctions in ZS-0 specimen, as shown in Fig. 4a. Additionally, the pores are gradually decreased with increasing the W content, as shown in Fig.4b–4d. It is worth mentioning that the diffusion mechanism of grains with intergranular pores is mainly the grain boundary migration during SPS process[29]. However, the diffusion mechanism after pore closure changes to grain boundary sliding, which further promotes the composite densification[30]. Therefore, the introduction of W element can reduce porosity and improve densification for ZrB_2-SiC ceramic composites.

The average grain size (equivalent grain diameter) of ZrB_2 in specimens with different W contents is shown in Fig. 5a. Fig. 5b and 5c show the typical characteristics of grain morphology of ZS-0 and ZSW-3 specimens, respectively. The ZrB_2 sizes of ZS-0, ZSW-1, ZSW-3, and ZSW-5 specimens are 5.1±0.5 μm, 4±0.4 μm, 3.1±0.3 μm, and 2.9±0.4 μm, respectively. Clearly, the average grain size is decreased significantly with increasing the W content from 0vol% to 5vol%. The microstructure of ZSW-3 specimen (Fig. 4c) shows that WB grains are uniformly distributed in ZrB_2 matrix, and most WB grains present the intergranular distribution. The WB particles as the pinning center of ZrB_2 grain boundary hinder the grain boundary migration, inhibit the coarsening of ZrB_2 grains, and improve the driving force for further composite densification. Therefore, W addition has dual-influence: promoting the composite densification and inhibiting the grain growth.

The ZrB_2 grains form a special core-shell structure in ZSW-3 specimen, as shown in Fig. 6. Similar structures can be found in ZrB_2-based ceramics with the addition of W-containing compounds[13]. This structure consists of in-situ formed solid solution (Zr, W)B_2 (shell) and the initial ZrB_2 grains (core). In this research, the core-shell structure is

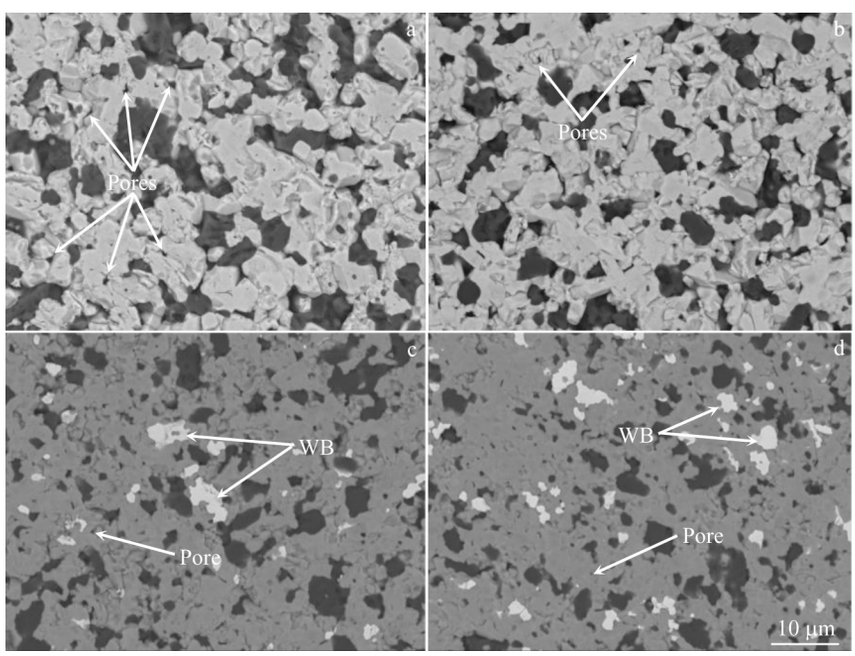

Fig.4 SEM morphologies of polished surfaces of ZS-0 (a), ZSW-1 (b), ZSW-3 (c), and ZSW-5 (d) specimens

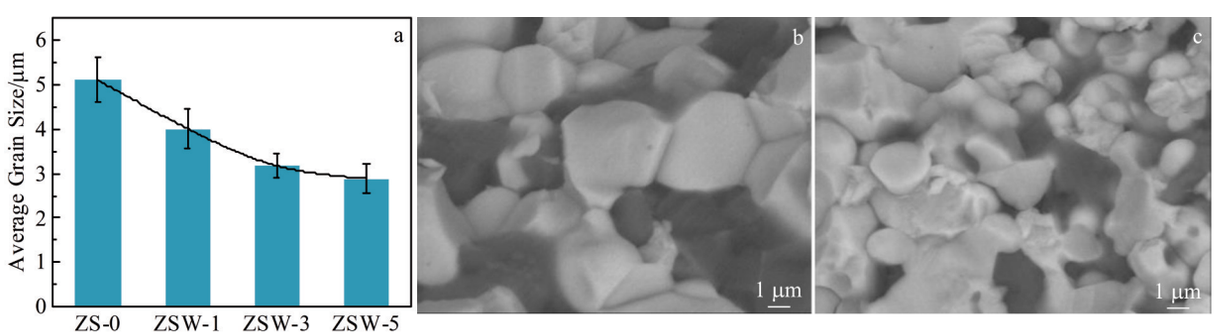

Fig.5 Average grain sizes of ZrB_2 in specimens with different W contents (a); SEM fracture morphologies of ZS-0 (b) and ZSW-3 (c) specimens

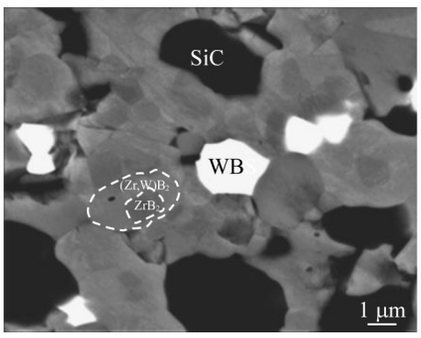

Fig.6 SEM morphology of ZSW-3 specimen with core-shell structure

formed in W-doped specimens. The eutectic temperatures of W-B system are 1930 – 2600 ° C. The introduction of Zr element can decrease the eutectic temperatures for the W-B system, which contributes to the generation of transient liquid phase and the enhancement in mass transfer mechanism during densification[18]. The transient liquid phase forms the core-shell structure after cooling. In this case, the transient liquid phase is considered as the main carrier for solute atoms to realize the grain boundary diffusion, which promotes the dissolution-diffusion behavior in the whole densification process. Therefore, the formation of core-shell structure results in higher density of W-doped specimens, compared with that of W-free specimens.

In this research, it is assumed that the reactions between ZrB_2 and W have two stages in the densification process, as shown in Fig.7.

The first stage is that the boron in ZrB_2 lattice diffuses into W to form the boron defects (ZrB_{2-x}) and WB, owing to the larger diffusion coefficient of boron in ZrB_2 lattice than that of W in the low temperature stage. The second stage is that the WB gradually dissolves in ZrB_{2-x}, resulting in the generation of transient liquid phase (Zr, W)B_2 at high temperatures[25]. The dissolution-diffusion behavior of W atom causes the lattice distortion of ZrB_2. The formation of boron defects (ZrB_{2-x}) and the transient liquid phase (Zr, W)B_2 leads to the decrease in ZrB_2 lattice, owing to the smaller covalent bond length of W (0.138 nm) than that of Zr (0.157 nm)[31]. In addition, the W content has a significant effect on WB

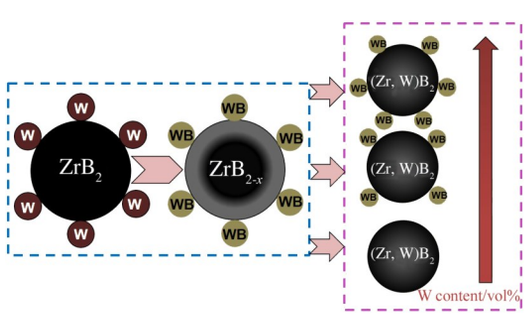

Fig.7 Schematic diagram of reactions between ZrB_2 and W during SPS process

dissolution in the second stage. According to the diffraction peak intensity of WB in Fig. 3, the WB phase is completely dissolved in ZrB_{2-x} when W content is 1vol% , and the dissolution of WB in ZrB_{2-x} reaches saturation when the W content increases to 3vol% . Therefore, the undissolved WB phases remain in the composites, and they can be clearly detected in ZSW-3 and ZSW-5 specimens by XRD. The densification process is inhibited with increasing the W content to 5vol% , indicating that the excessive WB phases may bring negative effects on the densification of composites. As for the 3vol% W-doped composites, the densification and microstructure of composites are significantly ameliorated, owing to the dissolution-diffusion of W and the formation of core-shell structure.

2.2 Mechanical properties

Fig. 8 shows the mechanical properties of ZrB_2-SiC-based composites with different W contents. Compared with the W-free specimen, the W-doped specimens show higher hardness, larger flexural strength, and higher fracture toughness. The hardness, strength, and toughness of composites are remarkably improved with increasing the W content from 1vol% to 3vol% , and then decreased slightly with further increasing the W content to 5vol% . The ZSW-3 specimen exhibits the highest hardness, flexure strength, and fracture toughness of 18.68±1.8 GPa, 600.8±30 MPa, and 7.84±0.8 MPa·$m^{1/2}$, respectively. The change in mechanical properties of ZrB_2-SiC-based composites is caused by the following factors. (1) The grain size and relative density play vital function in the mechanical behavior of polycrystalline ceramics[32]. As shown in Fig. 2 and Fig. 5, the relative density and mechanical properties have the similar variation trends with increasing the W content. The grain sizes are reduced after the W addition. The grain refinement and composite densification exert a complementary effect on the mechanical properties of W-doped composites. (2) The hardness of the ZrB_2, SiC, and WB main phases in ceramic composites is 23, 20, and 30 GPa, respectively[33]. The W-doped specimens are strengthened by the formed WB hard phases. (3) The strength improvement of W-doped specimens can be attributed to the formed core-shell structure. The dislocation chains are formed at the core/shell interfaces due to the core/shell thermal expansion mismatches after SPS process. The mechanical energy is absorbed by the dislocation motion, and the increase in dislocation density promotes the formation of sub-grains. The defect size decreases from micron scale (original grains) to nanometer scale (dislocation tangles) [34].

The crack paths of ZS-0 polished specimen are shown in Fig.9a. Only the crack deflections can be observed in the ZS-0 specimen. Different coefficients of thermal expansion (CTEs) of ZrB_2 in *a*-axis (6.9×10^{-6} K^{-1}) as well as *c*-axis (6.7×10^{-6} K^{-1}) and the CTE mismatch between ZrB_2 and SiC (*a*-axis=4.3×10^{-6} K^{-1}, *c*-axis=4.7×10^{-6} K^{-1}) all result in the residual stress at ZrB_2-ZrB_2 and ZrB_2-SiC interfaces. Therefore, the crack deflection is located at the ZrB_2-ZrB_2 and ZrB_2-SiC interfaces in ZS-0 specimen. The crack paths of 3vol% W-doped specimen are shown in Fig. 9b. The crack deflection, crack

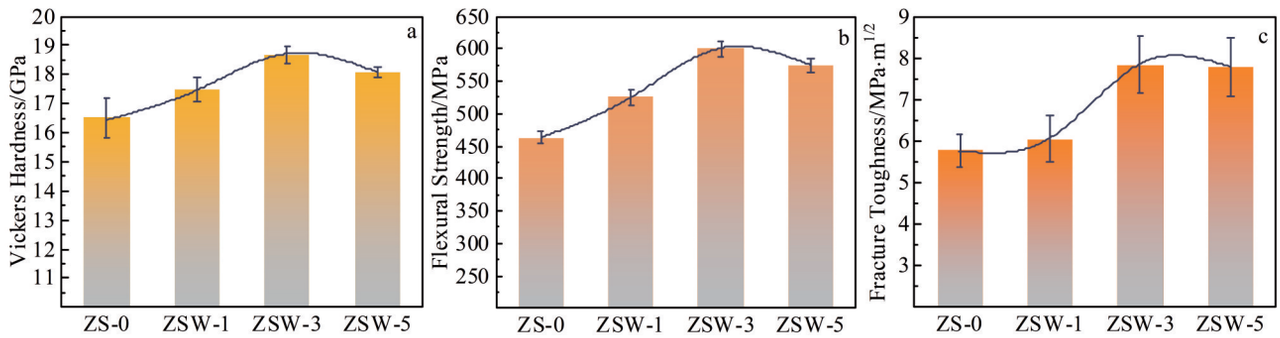

Fig.8 Vickers hardness (a), flexural strength (b), and fracture toughness (c) of ZrB_2-SiC-based composites with different W contents

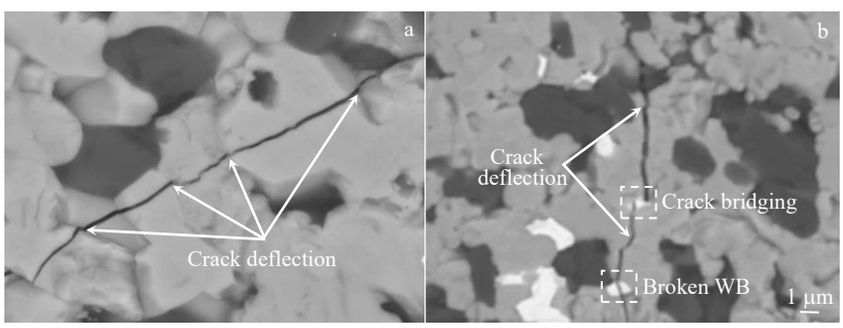

Fig.9 SEM morphologies of crack paths and toughening mechanism of ZS-0 (a) and ZSW-3 (b) specimens

bridging, and breakage of WB can be observed in the 3vol% W-doped specimen. The crack deflection of ZSW-3 specimen is also caused by the introduction of residual stress at ZrB_2/SiC/WB interface. The crack bridging is caused by the interactions of cracks with the third phases (WB and (Zr, W)B_2), which can effectively inhibit the crack propagation by energy absorption. In addition, the breakage of WB grains (Fig. 9b) can also absorb the energy of crack propagation. The coupling effects of crack deflection, crack bridging, and WB grains breakage significantly improve the fracture toughness of W-doped composites.

2.3 Oxidation behavior

Fig. 10 and Fig. 11 show SEM cross-section morphologies and EDS element distribution maps of different specimens after oxidation for 2 h.

As indicated by the dotted lines in Si distribution map in Fig.11a, the Si distribution is discontinuous and the Si amount is limited. The SiC deletion is obvious in the ZS-0 specimen. According to EDS results, it is found that the oxide scales consist of two distinct layers: the silica-rich layer (SiO_2 glass phase) and the SiC-depleted layer. The bright spots of ZrO_2 exist inside the SiO_2 glass layer of ZS-0 specimen, which lead to the formation of micro-voids and provide the direct channel for oxygen diffusion into the unreacted materials. Fig. 10b – 10d show SEM fracture morphologies of ZSW-1, ZSW-3, and ZSW-5 specimens after oxidation for 2 h, and Fig. 11b shows EDS results of ZSW-5 specimen after oxidation for 2 h. The thickness of SiC-depleted layer is reduced significantly with increasing the W addition amount. No obvious SiC-depleted layer can be observed when the W content is 5vol%. The W addition leads to the disappearance of SiC-depleted layer in W-doped specimens. Pan et al[35] found the similar results that the W and W-containing compounds can reinforce the ZrB_2-based composites. Fig. 12 shows the variation trends of oxide layer thickness (silica-rich layer+SiC-depleted layer) and oxidation mass gain with increasing the W addition amount. The oxide layer thickness and oxidation mass gain are gradually decreased with increasing the W content. The ZSW-5 specimen exhibits the lowest mass gain of about 4.5 mg·cm^{-2} and the thinnest thickness of about 10.5 μm among all specimens. Therefore, the W addition can ameliorate the oxidation resistance of the W-doped composites.

The formation of oxidation products is crucial to the oxidation behavior of boride ceramics. The W-doped composites can react with oxygen at 1500 °C and the related reactions are as follows:

$$ZrB_2\ (s)+5/2O_2\ (g)=ZrO_2\ (s)+B_2O_3\ (l) \quad (3)$$

$$SiC\ (s)+3/2O_2\ (g)=SiO_2\ (l)+CO\ (g) \quad (4)$$

$$SiC\ (s)+2O_2\ (g)=SiO_2\ (l)+CO_2\ (g) \quad (5)$$

$$SiC\ (s)+O_2\ (g)=SiO\ (l)+CO\ (g) \quad (6)$$

$$2WB\ (s)+3/2O_2\ (g)=2W\ (s)+B_2O_3\ (l) \quad (7)$$

$$WB\ (s)+9/2O_2\ (g)=2WO_3\ (s)+B_2O_3\ (l) \quad (8)$$

According to the volatility diagram of WB, WB can be oxidized into W and WO_3 at the low oxygen partial pressure and the high oxygen partial pressure, respectively[16,35]. The existence of oxidation product W can increase the thermal conductivity of the W-doped specimens, because the thermal conductivity of W (130 W·m^{-1}·K^{-1}) is higher than that of ZrB_2 (58 W·m^{-1}·K^{-1}). Thus, the surface temperature of W-doped

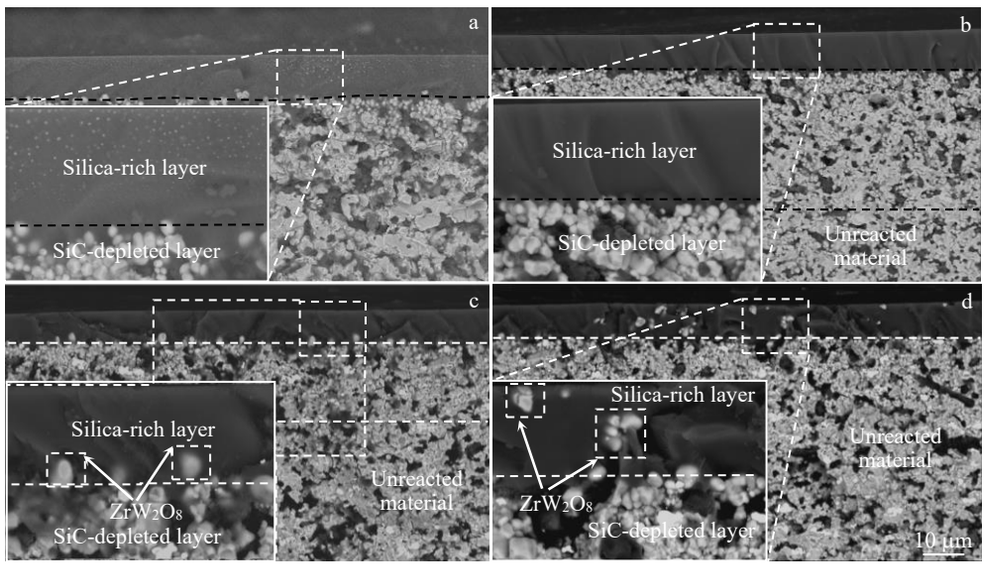

Fig.10 SEM cross-section morphologies of ZS-0 (a), ZSW-1 (b), ZSW-3 (c), and ZSW-5 (d) specimens after oxidation for 2 h

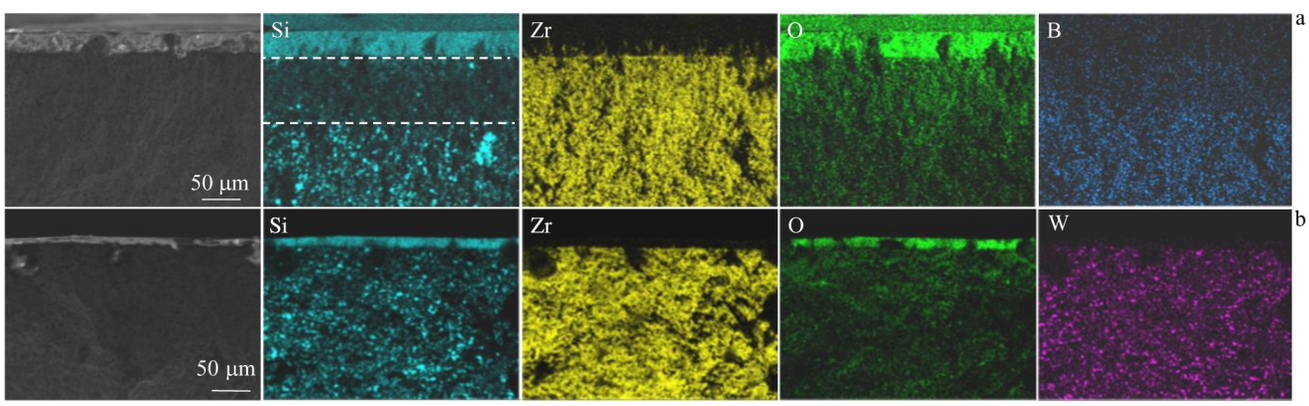

Fig.11 SEM images and EDS element distribution maps of ZS-0 (a) and ZSW-5 (b) specimens after oxidation for 2 h

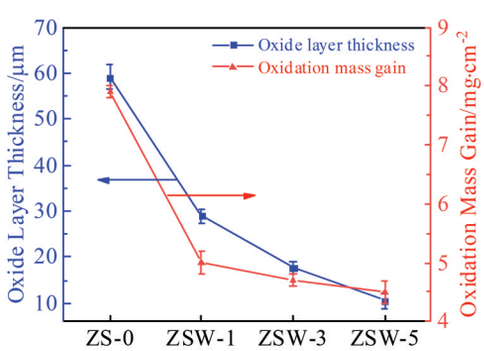

Fig.12 Oxide layer thickness and oxidation mass gain of ZrB_2-SiC-based composites with different W contents

specimens decreases during oxidation process. The decrease in surface temperature can retard the oxidation process of W-doped specimens[35]. In addition, the high temperature leads to the evaporation and escape of liquid and gas oxidation products. In the W-doped composites, the liquid phase oxidation products (B_2O_3, SiO_2, and WO_3) can be easily volatilized owing to the low melting points of composites in the oxidation process. The liquid phase WO_3 escapes in the gas form of WO_3, $(WO_3)_2$, $(WO_3)_3$, and $(WO_3)_4$. It is reported that the vapor pressure of tungsten oxide is lower than that of B_2O_3 at the oxidation temperature in this research, resulting in the more severe volatilization of tungsten oxide than that of B_2O_3[16]. A large amount of heat can be carried away by the volatilization of WO_3 molecules, thereby reducing the surface temperature of specimens. The reduction in surface temperature results in the fact that the W-doped specimens suffer from less severe oxidation. Additionally, the presence of WB can remarkably slow the volatilization rate of borosilicate phase[35]. Therefore, compared with the W-free specimens, the W addition is beneficial to reduce the oxide scale thickness and decrease the mass gain of W-doped specimens during oxidation process.

The W addition also results in the reduction in SiC-depleted layer. This is because the reduction in surface temperature can effectively hinder the further oxidation of the substrate layer. In addition, the generation of SiC-depleted layer is mainly attributed to the active oxidation of SiC into SiO and SiO_2.

WB can be oxidized into W and WO_3, as expressed by Eq.(7) and Eq.(8), respectively. There is a competition between the WB oxidation and SiC active oxidation during the oxidation process, which contributes to the effective hindrance of the generation of SiC-depleted layers. Therefore, the disappearance of SiC-depleted layer is attributed to the high content of WB in ZSW-5 specimen.

In this research, the SiO_2 and B_2O_3 form the borosilicate liquid phase at high temperatures. The formation of borosilicate liquid phase layer on the surface is vital to enhance the oxidation resistance of composites[33,35]. The formation of the dense borosilicate layer can effectively protect the material from further oxidation[16]. The proper amount of W addition can improve the stability of borosilicate liquid phase layer during the oxidation process. Besides, the appropriate dissolution of oxidation products WO_3 can significantly increase the viscosity and reduce the volatilization rate of borosilicate glass layer, which can effectively hinder the transmission of oxygen into the interior, thereby improving the oxidation resistance. Although WB and SiC can hardly react with each other, the reactions between their oxides are highly possible during the high-temperature oxidation[36]. Si and W elements can combine to form WSi_2[37]. During the further oxidation, some reactions may occur, as follows:

$$5WSi_2\ (s)+7O_2\ (g)=W_5Si_3\ (s)+7SiO_2\ (l) \quad (9)$$

$$W_5Si_3\ (s)+3O_2\ (g)=5W\ (s)+3SiO_2\ (l) \quad (10)$$

It is obvious that the WSi_2 and W_5Si_3 can react with oxygen to form SiO_2 phase during the high-temperature oxidation, which complements the volatile SiO_2 glass phase. Therefore, more SiO_2 phases can be used to impede the oxygen diffusion and effectively improve the oxidation resistance.

The (Zr, W)B_2 shell and WB widely exist in W-doped specimens and the oxidation products are mainly composed of ZrO_2 (s), W (s), WO_3 (l), and B_2O_3 (l, g). Based on the ZrO_2-WO_3 phase diagram, the appropriate amount of WO_3 can lead to the eutectic reaction between ZrO_2 and WO_3 at 1231 °C[21]. Therefore, the liquid phase is formed under the oxidation conditions at 1500 °C. The liquid phase is capable to fill the micro-voids during oxidation process, leading to the formation of dense oxide layers[13]. The bright phases ZrW_2O_8 generated by the eutectic reaction between ZrO_2 and WO_3 are found inside the oxide layers. With the negative CTE, ZrW_2O_8 is beneficial to reduce the defects in the oxide layer[35]. The dense oxide layer can prevent the oxygen diffusion into the unreacted material. In addition, the field strength of cation can significantly change the molecular arrangement of SiO_2 phase by attracting the surrounding non-bridging oxygen[38]. The existence of W^{6+} cation with relatively high field strength (0.1667 nm^{-2}) can separate the SiO_2 glass phase and consequently increase the viscosity of SiO_2 glass phase. The oxide layer with high viscosity can further prevent the oxygen diffusion and improve the oxidation resistance of W-doped specimens.

3 Conclusions

1) The W introduction can promote the formation of core-shell structure with original ZrB_2 grains as the core and in-situ formed (Zr, W)B_2 solid solution as the shell. The densification of W-doped composites is remarkably improved with increasing the W content from 1vol% to 3vol%, but it is slightly decreased with further increasing the W content to 5vol%. The average grain size is decreased significantly with increasing the W content from 0vol% to 5vol%.

2) The W addition can effectively improve the mechanical properties of W-doped composites. In addition to the densification, grain refinement, and in-situ formation of core-shell structure, the W addition also contributes to the coupling toughening mechanisms, such as WB breakage and crack bridging. The ZrB_2-SiC-based composite with 3vol% W exhibits the highest Vickers hardness (18.68±1.8 GPa), the highest flexural strength (600.8±30 MPa), and the highest fracture toughness (7.84±0.8 $MPa·m^{1/2}$).

3) The high-temperature oxidation behavior of the W-doped composites is gradually improved with increasing the W content from 1vol% to 5vol%. The 5vol% W-doped composite has the thinnest oxide layer (thickness of about 10.5 μm) and the lowest mass gain (4.5 $mg·cm^{-2}$). Additionally, the SiC-depleted layer disappears in this composite.

References

1 Liu C Q, Yuan X X, Wang W T *et al*. *Ceramics International*[J], 2022, 48(3): 4055

2 Gui K X, Zhang W H, Zhu D D *et al*. *Rare Metal Materials and Engineering*[J], 2020, 49(7): 2213

3 Wang P, Li S J, Wei C C *et al*. *Journal of Alloys and Compounds*[J], 2019, 781: 26

4 Gao Z T, Geng H M, Qiao Z H *et al*. *Ceramics International*[J], 2023, 49(4): 6409

5 Vorotilo S, Sidnov K, Kurbatkina V V *et al*. *Journal of Alloys and Compounds*[J], 2022, 901: 163 368

6 Derakhshandeh M R, Fazili A, Golenji R B *et al*. *Journal of Alloys and Compounds*[J], 2021, 887: 161 403

7 Silvestroni L, Sciti D. *Journal of the American Ceramic Society*[J], 2011, 94(6): 1920

8 Golla B R, Thimmappa S K. *Journal of Alloys and Compounds*[J], 2019, 797: 92

9 Nisar A, Bajpai S, Khan M M *et al*. *Ceramics International*[J], 2020, 46(13): 21 689

10 Thimmappa S K, Golla B R, Bhanu Prasad V V *et al*. *Ceramics International*[J], 2019, 45(7): 9061

11 Eatemadi R, Balak Z. *Ceramics International*[J], 2019, 45(4): 4763

12 Sengupta P, Sahoo S S, Bhattacharjee A *et al*. *Journal of Alloys and Compounds*[J], 2021, 850: 156 668

13 Zou J, Sun S K, Zhang G J *et al*. *Journal of the American Ceramic Society*[J], 2011, 94(5): 1575

14 Jarman J D, Fahrenholtz W G, Hilmas G E *et al*. *Journal of the European Ceramic Society*[J], 2022, 42(5): 2107
15 Kavakeb K, Balak Z, Kafashan H. *International Journal of Refractory Metals and Hard Materials*[J], 2019, 83: 104 971
16 Li C, Niu Y R, Zhong X *et al*. *Journal of the European Ceramic Society*[J], 2019, 39(15): 4565
17 Vaziri P, Balak Z. *International Journal of Refractory Metals and Hard Materials*[J], 2019, 83: 104 958
18 Monteverde F, Silvestroni L. *Materials & Design*[J], 2016, 109: 396
19 Krishnarao R V, Alam M Z, Das D K. *Corrosion Science*[J], 2018, 141: 72
20 Li Yizhen, Zhu Shizhen, Wang Hui *et al*. *Rare Metal Materials and Engineering*[J], 2020, 49(2): 533 (in Chinese)
21 Kazemzadeh D M, Fahrenholtz W G, Hilmas G E. *Corrosion Science*[J], 2014, 80: 221
22 Mohammadpour B, Ahmadi Z, Shokouhimehr M *et al*. *Ceramics International*[J], 2019, 45(4): 4262
23 Wang H, Chen D, Wang C A *et al*. *International Journal of Refractory Metals and Hard Materials*[J], 2009, 27(6): 1024
24 Yung D L, Antonov M, Hussainova I. *Ceramics International*[J], 2016, 42(11): 12 907
25 Ding H J, Wang X G, Xia J F *et al*. *Journal of Alloys and Compounds*[J], 2020, 827: 154 293
26 Pourmohammadie V N, Nayebi B, Shahedi A M *et al*. *Ceramics International*[J], 2016, 42(2): 2724
27 Silvestroni L, Meriggi G, Sciti D. *Corrosion Science*[J], 2014, 83: 281
28 Zhang Y, Guo W M, Jiang Z B *et al*. *Scripta Materialia*[J], 2019, 164: 135
29 Nisar A, Ariharan S, Balani K. *International Journal of Refractory Metals and Hard Materials*[J], 2018, 73: 221
30 Lu K. *International Materials Reviews*[J], 2013, 53(1): 21
31 Shen Y B, Wang X G, Zhang G J *et al*. *Journal of the American Ceramic Society*[J], 2019, 102(6): 3090
32 Gu M, Huang C, Zou B *et al*. *Materials Science and Engineering A*[J], 2006, 433(1–2): 39
33 Vedel D, Grigoriev O, Mazur P *et al*. *Journal of Alloys and Compounds*[J], 2021, 879: 160 398
34 Silvestroni L, Sciti D. *Journal of Alloys and Compounds*[J], 2014, 602: 346
35 Pan X H, Li C, Niu Y R *et al*. *Corrosion Science*[J], 2020, 168: 108 560
36 Zou J, Virtudes R, Jon B. *Acta Materialia*[J], 2017, 133: 293
37 Fan Yan, Fan Jinglian, Li Wei *et al*. *Materials Science and Engineering of Powder Metallurgy*[J], 2016, 21(5): 755 (in Chinese)
38 Jayaseelan D D, Zapata S E, Chater R J *et al*. *Journal of the European Ceramic Society*[J], 2015, 35(15): 4059

添加W对ZrB_2-SiC复合材料的微观组织、力学性能和氧化行为的影响

高中堂[1]，卢佳炜[1,2,3]，于　源[2,3,4]，王毅飞[5]，余德锋[1]，李彤阳[2,3]，王鲁杰[2,4]，汤华国[2,3]，乔竹辉[2,3,4]
(1. 西安科技大学 机械工程学院，陕西 西安 710054)
(2. 中国科学院 兰州化学物理研究所 固体润滑国家重点实验室，甘肃 兰州 730000)
(3. 烟台先进材料与绿色制造山东省实验室，山东 烟台 264006)
(4. 烟台中科先进材料与绿色化工产业技术研究院，山东 烟台 264006)
(5. 西北有色金属研究院，陕西 西安 710016)

摘　要：通过放电等离子烧结技术制备了添加不同W含量(1%，3%和5%，体积分数，下同)的ZrB_2-SiC复合材料，研究了烧结过程中复合材料的致密化行为，分析了添加W对复合材料微观组织演化、相组成、力学性能和氧化行为的影响。结果表明：W的添加使复合材料的微观组织表现出核壳结构，以ZrB_2晶粒为核，原位形成的(Zr, W)B_2固溶体为壳，有效地促进了复合材料的致密化和晶粒细化。对比不含W的复合材料，含W复合材料的维氏硬度、抗弯曲强度和断裂韧性显著提高，W添加含量在3%时力学性能最优，复合材料表现出最佳的硬度、强度和韧性。随着W添加量从0%增加到5%，复合材料的氧化增重和氧化层厚度逐渐减小。当W添加量为5%时，复合材料的SiC贫化层消失。最后，详细说明了W的添加对复合材料性能的影响机制。

关键词：ZrB_2-SiC复合材料；致密化；微观组织；力学性能；氧化行为

作者简介：高中堂，男，1983年生，博士，副教授，西安科技大学机械工程学院，陕西 西安 710054，电话：029-85583159，E-mail：zhongtanggao@xust.edu.cn